Drivers of dissolved organic matter in estuarine porewater under ultramafic watershed influence

Mouras N.[1], Mounier S. [2], Meyneng M. [3], Antypas F. [1], Haize T. [1*], Oursel B. [4], Magoni-Laporte C. [5], Siano R. [4], Lemonnier H. [1]

Affiliation when the works was conducted:

[1] Ifremer, CNRS, IRD, Univ Nouvelle-Calédonie, Univ La Réunion, ENTROPIE, F-98800 Nouméa, Nouvelle-Calédonie, France

[2] *Université de Toulon, Aix Marseille Univ., CNRS, IRD, MIO, Toulon, France*

[3] French Institute for Research in the Science of the Sea (IFREMER), DYNECO, BP70 Plouzané, France

[4] *Aix Marseille Univ, Université de Toulon, CNRS, IRD, MIO, Marseille, France*

[5] Institute of Exact and Applied Sciences (ISEA EA7484), University of New Caledonia, Nouméa, France

Present address when different:

* European Molecular Biology Laboratory (EMBL), Heidelberg, Germany

Abstract

Dissolved organic matter (DOM) in a tropical estuarine ecosystem was characterized through the analysis of optical properties of coloured and fluorescent matter in porewater samples collected from the coastal areas of New Caledonia (South-West Pacific Ocean). Surface sediment porewaters were analysed in five sites under the influence of catchment areas characterized by different proportions of ultramafic soils. Four main components were identified, comprising both autochthonous and allochthonous materials across all sites. Significant site-specific effects were driven by three main factors: geology, catchment area size, and mangrove presence. Ultramafic sediments impacted more or less by mining activities resulted in low coloured dissolved organic matter content and high

biological activity. Larger catchment areas led to high concentrations of terrestrial humic-like and fulvic-like compounds. The presence of mangroves influenced the abundance of humic-like-mangrove compounds. More broadly, our research highlights the importance of considering the entire land-sea continuum and the complex interactions between terrestrial and marine ecosystems to fully understand the dynamics of estuarine environments.

Keys words: Porewater, Fluorescence spectroscopy, CDOM, Ultramafic environment, New-Caledonia, coastal environment

Acknowledgements:

This study was part of ECOMINE financed by the CRESICA (Consortium pour la recherche, l'enseignement supérieur et l'innovation en Nouvelle-Calédonie), as part of the "au fil de l'eau" program. We thank the IMAGO-LAMA team (IRD-Nouméa) for chemical analyses. We acknowledge the skippers and the nautical resources from E.G.L.E, Tarap Destination and the IRD. We would like to thank Quéré Robin and Schaefer Anne-Lou for their support and advise in QGIS and Python analysis.

Declaration of Interest statement:

The authors declare that they have no known competing financial interests or personal relationships that could have appeared to influence the work reported in this paper.

Corresponding authors information:

N. Mouras: naina.mouras@ifremer.fr

S.Mounier : stephane.mounier@univ-tln.fr

M. Meyneng: mathisse.meyneng@ifremer.fr

F. Antypas: florence.antypas@ifremer.fr

T. Haize: thomas.haize@embl.de

B.Oursel: benjamin.oursel@univ-amu.fr

C. Laporte-Magoni: christine.laporte@unc.nc

R. Siano: raffaele.siano@ifremer.fr

H. Lemonnier: hugues.lemonnier@ifremer.fr

Full contact details of the corresponding author:

Naïna Mouras naina.mouras@ifremer.fr
Ifremer New Caledonia,
101, Promenade Roger Laroque
B.P. 32 078
98897 NOUMEA CEDEX

Author's contribution

Naïna Mouras: Writing - Original Draft, Writing - Review & Editing, Investigation, Visualization, Methodology, Formal analysis. **Stéphane Mounier:** Validation, Writing - Review & Editing, Resources. **Mathisse Meyneng:** Writing - Review & Editing, Investigation. **Florence Antypas:** Investigation, Methodology. **Thomas Haize:** Investigation, Methodology. **Benjamin Oursel:** Writing - Review & Editing, Investigation, Resources. **Christine Magoni-Laporte:** Investigation, Writing - Review & Editing, Validation. **Raffaele Siano:** Conceptualization, Methodology, Investigation, Writing — review & editing, Supervision, Project administration. **Hugues Lemonnier:** Conceptualization, Methodology, Investigation, Writing — review & editing, Supervision, Project administration, Funding acquisition.

Drivers of dissolved organic matter in estuarine porewater under ultramafic watershed influence

ABSTRACT

Dissolved organic matter (DOM) in a tropical estuarine ecosystem was characterized through the analysis of optical properties of coloured and fluorescent matter in porewater samples collected from the coastal areas of New Caledonia (South-West Pacific Ocean). Surface sediment porewaters were analysed in five sites under the influence of catchment areas characterized by different proportions of ultramafic soils. Four main components were identified, comprising both autochthonous and allochthonous materials across all sites. Significant site-specific effects were driven by three main factors: geology, catchment area size, and mangrove presence. Ultramafic sediments impacted more or less by mining activities resulted in low coloured dissolved organic matter content and high biological activity. Larger catchment areas led to high concentrations of terrestrial humic-like and fulvic-like compounds. The presence of mangroves influenced the abundance of humic-like-mangrove compounds. More broadly, our research highlights the importance of considering the entire land-sea continuum and the complex interactions between terrestrial and marine ecosystems to fully understand the dynamics of estuarine environments.

Keys words: Porewater, Fluorescence spectroscopy, CDOM, Ultramafic environment, New-Caledonia, coastal environment

GRAPHICAL ABSTRACT

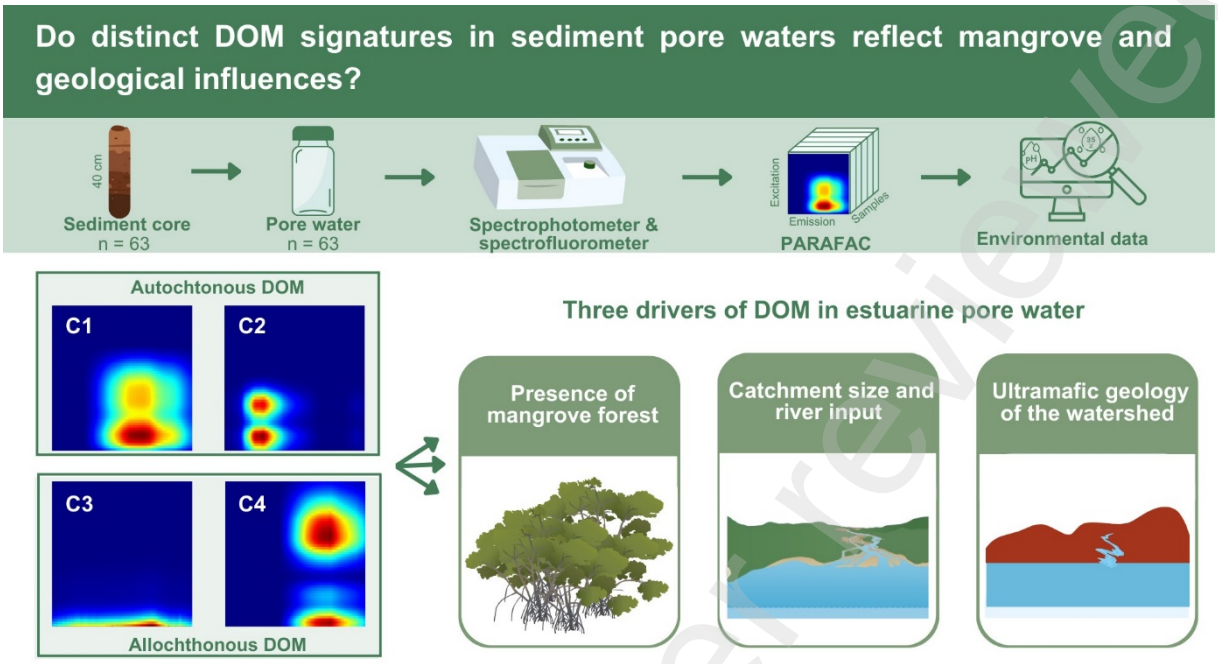

HIGHLIGHTS

- DOM in New Caledonia's estuarine ecosystems showed distinct optical signatures.
- Ultrabasic sites had low absorption and smaller molecules.
- Fluorescence varied with mangroves, catchment size, and geological conditions.
- Distinct optical signatures linked to site-specific environmental factors.

1. Introduction

Estuaries are essential in the global organic carbon cycle, functioning as a mixing zone interface between land and sea alongside river systems (Blair & Aller, 2012). The quantity and composition of organic matter (OM) within estuaries are fundamental drivers of biogeochemical processes and biological activity (Alongi, 1997). Organic matter is composed of diverse organic compounds sourced from various origins, including terrestrial inputs carried by rivers (Cai, 2011; Wu et al., 2023). This allochthonous material, influenced by the surrounding land, dynamically interacts with autochthonous organic matter produced within the estuarine environment.

In mangrove forest, autochthonous organic matter is produced through the decomposition of leaves and branches, enriching the litter with humic substances (Jaffé et al., 2004; Maie et al., 2008). Concurrently, due to high temperatures, biological processes actively contribute to the transformation of this organic substrate (Zhou et al., 2019). When OM remineralizes, it releases dissolved inorganic carbon and nutrients, accumulating within the porewater that could subsequently transported to adjacent ecosystems (Dittmar & Lara, 2001). Although many studies on OM outwelling, the OM cycles in tropical estuarine systems remain underexplored (Santos et al., 2021).

Analysing dissolved organic matter (DOM) in sediment porewater is valuable for identifying biogeochemical processes in estuarine systems, as it reflects sedimentary particulate OM remineralization resulting from significant fluxes between sediments and the water column (Burdige, 2001). Moreover, DOM in porewater is a useful proxy for identifying OM sources and determining the degree of environmental anthroponization (Burdige et al., 2004), and it provides insights into metal-DOM interactions (He et al., 2019). In fact, metals can interact with DOM, leading to organic complexes that play a crucial ecological role by enhancing their transfer, changing the metal speciation, and modifying the availability of metal in aquatic ecosystems (Mounier et al., 2011; Wu et al., 2011). Lateritic soils resulting from ultrabasic rocks alteration, characterized by their naturally high concentrations of metals such as Ni, Mn, and Co, may raise questions due to their potential to complex with OM. In tropical climates, alteration is more significant and metallic impact from ultramafic soil can be enhanced (Kierczak et al., 2021).

Beyond quantitative methods for measuring dissolved organic carbon (DOC) concentration, analysing the light-absorbing fraction of DOM offers qualitative insights into its distribution. Optical properties, such as Coloured Dissolved Organic Matter (CDOM) and Fluorescent Dissolved Organic Matter (FDOM), are commonly used to characterize DOM and provide insights into sources and complex interactions within environments (Coble et al., 1998). The major fluorophores observed in sediment porewater are humic-like compounds and protein-like compounds such as tryptophan and tyrosine (Burdige, 2001; Burdige et al., 2004).

While studies on DOM in the water column are abundant (e.g. Coble, 1996 ; Nelson & Siegel, 2013), fewer studies have focused on sediment porewaters in recent years and particularly in tropical ecosystems (Chen & Hur, 2015). This study aimed to investigate the composition and origin of DOM in sediment porewaters to discover distinctive signatures resulting from the interplay of metal-rich geology and mangrove-derived organic contributions. The main objective was to elucidate how mangrove and geological conditions drive organic matter dynamics in tropical ecosystems, focusing on surface sediment at the land-sea interface.

2. Material and methods

2.1. Study area and sampling strategy

New Caledonia is a mountainous archipelago located in the south-western Pacific Ocean (Fig.1). Its geology is complex and composed of peridotite nappe, ophiolitic units, volcaniclastic sedimentary rocks, and metamorphic terranes (Maurizot et al., 2020). The northern part of the East Coast is under metamorphic influence, while the large southern massif is ultramafic, as well as much of the west coast; the central part is composed of sedimentary and magmatic rocks. The tropical climate, influenced by the Intertropical Convergence Zone (ITCZ) and South Pacific Convergence Zone (SPCZ), results in distinct wet and dry seasons (Vincent, 1994), can lead to substantial rainfall. During our sampling campaign, New Caledonia experienced a “La Niña phase”, indicated by the Oceanic Niño Index (ONI) of -1.1 (NOAA, V5 2023).

Water flows from land to sea through around a hundred rivers (Fichez et al., 2010). Mangroves cover over 80 % of the west coast of New Caledonia and 20 % of the east coast with rich biodiversity (Marchand et al., 2012) face anthropogenic pressures from aquaculture, urbanization, and mining (Bourgeois et al., 2020; Dubuc et al., 2024; Robin et al., 2022). Urban development remains sparse, concentrated mainly in Nouméa, with average population density of 15 people/km² (Payri et al., 2018).

Porewater samples were collected from five estuaries (Fig. 1), chosen to represent coastal environments near river mouths with varying geological and mangrove cover. Each area included three to five sampling stations (a, b, c, d, e), with three replicates per station, totalizing sixty-three sediment

86 samples. This approach aimed to capture maximum variability across multiple scales: micro-scale
87 (replicates), local scale (within-site variation), and regional scale (between the five areas).

88 The Pirogue site (P) is located within the Pirogue River estuary, covering a watershed area of 147.9
89 km², composed predominantly (99.9%) of ultramafic sediments (Lalau et al., 2019). This region, part of
90 South New Caledonia's Grand Massif ultramafic zone, is known for high metal concentrations (Ni, Co,
91 Mn, Cr) in river waters from suspended solids (Bird et al., 1984). Lateritic clasts, identifiable by their
92 red colour, often become visible post-rainfall, forming mudflats (Fernandez et al., 2017). The Pirogue
93 estuary lacks mangrove forests, agricultural activities, and has low human density.

94 The Coulée area (C), where the proportion of ultramafic sediments stands at 99.8%, is situated near
95 the mouth of the Coulée River, covering a catchment area of 84.4 km² (Lalau et al., 2019). The
96 watershed exhibits a land cover of 26% forest, 54% savannah, and 9% mining sites (Desclaux et al.,
97 2018), with a sparse mangrove cover. The municipality of Mont-Dore, near the site of La Coulée,
98 features agricultural activity and residential areas.

99 Dumbéa (D) area with a proportion of ultramafic sediments amounting to 75.8%. The catchment area
100 of the Dumbéa river is substantial totalling 218.7 km² (Lalau et al., 2019). The estuary is bordered by a
101 mangrove. Previous study had suggested a low residence time of seawater in Dumbéa Bay, resulting
102 in rapid transformations of the surficial sediments (Ambatsian et al., 1997). Poultry farming, a golf
103 course, and human habitations are located upstream of the estuary, and an oyster farming operation
104 is situated at the river mouth.

105 The Voh-Koné-Pouembout area (VKP), characterized by some watersheds with 100%
106 ultrabasic/lateritic substrates and some catchments mixing 62.61% volcano-sedimentary and 37.39%
107 ultramafic, is situated between the Voh River and the Coco River estuaries. Spanning a significant
108 catchment area of 260.3 km² (Lalau et al., 2019), this region features a landscape dominated by a dense
109 mangrove forest. Close to, the Koniambo massif has been an active nickel mining site since the late

19th century. This area in the Northern Province has a low number of habitations and few agricultural activities.

The Ouegoa area (O), distinguished by a 0.7% proportion of ultramafic sediments in its watershed, is situated near the Diahot River, the largest river in New Caledonia, extending 90 km in length (Bird et al., 1984) with a catchment area of 459.9 km² (Lalau et al., 2019). Situated at the top of the "Grande Terre Island", the estuary of Ouegoa is surrounded by land and extensive mangroves (Bird et al., 1984). Its geological composition consists in volcano-sedimentary metamorphized rocks (blueschists, greenschists and eclogites grades) (Lillie & Brothers, 1970; Maurizot et al., 2020). This area has a sparse population engaged in family agricultural activities.

2.2. Field sampling

Undisturbed large sediment cores (40 cm long and 10 cm in diameter) with overlying water were collected by a diver using a manual plastic corer to minimize sediment disturbance, focusing on muddy sediments, as these habitats better to preserve organic matter.

Surface water salinity and temperature (0-30 cm) were measured from the boat using a tetracon 325 sensor. Sediment physicochemical parameters (pH, temperature, and redox potential [Eh]), were measured *in situ* at -1.5 cm depth using specific sensors: pH with a 3320 WTW® SenTix® 81 glass electrode, and Eh with a SenTix® ORD WTW® pH315i electrode, allowing for stable readings after a minimum of 30 minutes, with electrodes rinsed between samples to prevent measurement errors.

Porewater was extracted at -1.5 cm depth using Rhizon® sediments moisture samplers (pore size 0.2 µm) inserted directly into pre-drilled holes within the corer. An average of 10 mL of porewater from each Rhizon® was collected using a pressurized syringe, filtered through 25 mm of diameter glass filters (Whatman GFF, 0.7 µm) previously combusted (450 °C, 6h) for dissolved organic carbon (DOC) analysis, and stored at +4 °C in pre-cleaned 24 mL glass tubes (Wheaton) with acidification using 12 M HCl (pH < 2). For dissolved organic matter (DOM) analysis, 10 mL of extracted porewater was transferred to

glass vials cleaned with 10% HCl, rinsed with Milli-Q water, and combusted (450 °C, 6 h) before storage at +4 °C in darkness.

Sediment sampling involved carefully collecting an average of 30 g from the top 3 cm using a Teflon spoon after porewater extraction. Portions were transferred to polypropylene vials for total metals analysis and to petri dishes for porosity, water content, and particle size measurements. The details of the sampling stations, are provided in Table A1.

2.3. Analytical methods

Sediment samples were analysed to understand their composition and properties. Particle size distribution was characterized using the Malvern Mastersizer Hydro 2000S laser diffraction analyser (university of New Caledonia), providing insights into grain size and component distribution. Mineralogical composition was determined by X-Ray Diffraction (XRD) using a PANalytical AERIS XRD Diffractometer with a Co source. Sediment water content was expressed as a percentage of wet weight after air drying.

The Walkley & Black method quantified total organic carbon (TOC) via wet oxidation (Ulmer et al., 1992). Metal concentrations were analysed post-alkaline fusion, using Inductively Coupled Plasma Optical Emission Spectroscopy (ICP OES).

Porewater salinity was measured with a refractometer in lab, and DOC concentrations with a Shimadzu TOC-VCSH carbon analyser. CDOM measurements were performed using a Shimadzu UV-1700 spectrophotometer at 200-700 nm, with data acquisition by Uvprobe software. To avoid contamination, the quartz cell was rinsed with 10% HCl and Milli-Q water between samples. Absorption coefficients and indicators, including spectral slopes (S275-295), and SR were calculated to differentiate marine and terrestrial CDOM sources (Hansen et al., 2016), and provided information about the molecular weight (Helms et al., 2008).

Fluorescence analyses were performed using a PERKIN ELMER LS 55 spectrofluorometer with excitation wavelengths from 200 to 500 nm and emission measurements from 280 to 550 nm every 5

nm. Samples were brought to room temperature (+ 20°C) and transferred to a pre-washed 2 mm optical path quartz cell (Hellma Micro-cuvette 10 x 2 mm). The cell was rinsed with 10% HCl, Milli-Q water, and the sample itself before each analysis.

The Excitation-Emission Matrix (EEM) technique generated 3D map of fluorophore composition (Coble, 1996) analysed using parallel factor analysis (PARAFAC) with ProgMEEF software (Mediterranean Institute of Oceanography (MIO) - Université de Toulon, 2018) through MATLAB R2017a software. A modified version of ProgMEEF (April 2022) was developed (© Roland Redon MIO – Université de Toulon) to accommodate the analysis of samples using an asymmetric 2 mm-10 mm optical path cell.

EEM data were normalized by Raman scattering peak of pure water at Ex/Em = 275/303 (Coble, 1996) to eliminate instrumental variation and enable interlaboratory comparison (Zepp et al., 2004). Decomposition used the CORCONDIA (CORe CONsistency DIAgnostic) diagnostic to determine model validity, selecting higher components number with a CORCONDIA value over 60%. These components were compared with existing literature. Various fluorescence indexes such as BIX (biological index) (Parlanti et al., 2000), and HIX (humification index) (McKnight et al., 2001) were calculated from the 3D fluorescence spectra to characterize the material's source.

2.4. Statistics

Statistical analyses were performed using R version 4.0.3. A significance level of $p < 0.05$ indicated statistical significance. The Kruskal-Wallis test assessed differences between sites and stations due to non-normality and heteroscedasticity, followed by Wilcoxon tests for pairwise comparisons if significant differences were found. PCA examined the influences of physico-chemical parameters, granulometry, and metal concentrations, with data center-reduced to address heterogeneity. Spearman's correlation matrix was used for the PCA analysis due to non-normal data distribution.

3. Results and discussion

3.1. Environmental conditions drivers

Despite being widely dispersed geographically at the New Caledonia scale, these study sites exhibited striking environmental similarities. As expected, they shared common granulometric conditions with no significant differences observed either within each site or between stations of the same site (Fig. A1). However, they distinguished themselves significantly by the mineralogy of their substrates, encompassing ultramafic, volcano-sedimentary, and metamorphic soils (Lillie & Brothers, 1970).

In fact, the samples have been categorized based on the detected minerals (XRD data), providing valuable insights into the site geology (Fig. A2). Ultramafic laterites stood out with the presence of Goethite (FeOOH) and Willemseite ($Ni_3Si_4O_{10}(OH)_2$), highlighting the iron and nickel rich nature of these weathering resulting soils (lateritic nickel ore). Glaucophane ($Na_2Mg_3Al_2Si_8O_{22}(OH)_2$) identifications confirm the contribution of metamorphic clasts in O sediments (metamorphic amphibole of the blueschist grade). The occurrences of albite (Na ($AlSi_3O_8$); a magmatic and metamorphic plagioclase) in the VKP and O sediments are consistent with the erosion of a volcano-sedimentary and metamorphized volcano-sedimentary rocks. The detection of Laumontite ($CaAl_2Si_4O_{12}$. $4H_2O$; Zeolite group) indicates previous surface hydration of volcanic glass in volcano-sedimentary rocks from the VKP site. Lastly, marine influence was evident through the detection of Pyrite (FeS_2) and Halite (NaCl) in samples from DD, VKP, and O. These mineralogies offered a comprehensive understanding of geological diversity and environmental processes at each site.

Distinct disparities in soil metal concentrations were observed among the sites (Fig. 2a, A2, Table A2). The concentrations of metals like Zn, Mn, Cr, Ni, Fe, and Co were strongly correlated (Spearman correlation). Ni and Cr concentrations were very high ranging between 15.5 ± 0.9 $mg.g^{-1}$ and 22.4 ± 4.1 $mg.g^{-1}$, and between 17.8 ± 1.2 $mg.g^{-1}$ and 20.1 ± 0.5 $mg.g^{-1}$ of [Cr], for P and C sites, respectively (Table A2). Thus, the high [Ni] and [Cr] concentrations are consistent with their dominant ultramafic geology. However, [Cr] at VKP (ranging from 1.4 ± 0 $mg.g^{-1}$ to 3.1 ± 4.1 $mg.g^{-1}$) and D (ranging from 2.5 ± 0 $mg.g^{-1}$ to 11.4 ± 2.7 $mg.g^{-1}$) are below the maximum levels found ultramafic sites of our study but still exceed the global median of 0.05 $mg.g^{-1}$ (Kierczak et al., 2021). Similar trends were observed for Ni, with the

highest concentrations at P and C sites, ranging from 4.2 ± 0.4 mg.g^{-1} (P-a) to 6.5 ± 0.2 mg.g^{-1} (C-b), followed by lower values at D (between 0.7 ± 0.1 mg.g^{-1} and 3.1 ± 0.2 mg.g^{-1}) and VKP ranging from 0.5 ± 0 mg.g^{-1} to 1 ± 0.4 mg.g^{-1}, and no Ni concentration upper the detection limit was measured at O.

The Si and Fe concentrations witness the geologic differences of the sampled sites. Along the ultrabasic alteration profile, Si concentrations rise while Fe concentrations increase. Hydrolysis reactions cause the destruction of ferromagnesian silicates, unstable under surface conditions, by solubilization of Si and Mg, which infiltrate to greater depths. Conversely, Fe, mostly in the form of very insoluble Fe^{3+}, remains in residual rocks, forming iron oxide and hydroxide crusts in the final stages of weathering (Dublet et al., 2015). Sediments derived from the erosion of ultrabasic regolith therefore have high [Fe] and relatively low [Si] concentrations compared with other rocks. In contrast, the metamorphic rocks in the O region are composed mainly of alumino-silicates and pure silicates, resistant to surface alteration. The sediments resulting from their erosion therefore have lower [Fe] but higher [Si] concentrations. Sediments from watersheds of mixed volcano-sedimentary and ultrabasic substrates have [Si] and [Fe] concentrations intermediate between the other sites. Volcanic rocks, mainly basaltic in these units, are also composed of ferromagnesium silicates, in lesser proportion than ultrabasic rocks, which explains the higher Fe concentrations than in the sediments from the O site.

Total organic carbon concentrations varied, with the lowest at P-b (10.90 ± 1.76 mg.g^{-1}) and the highest at D-b (61.9 ± 2.33 mg.g^{-1}). The P site lacks mangroves, whereas D-b is near mangroves (Fig. 1). Indeed, Fig. 2B shows higher TOC close to mangroves. DOC concentrations at sites closest to mangroves (Fig. 1), such as O (a, c, d, e), D (b), and VKP (d, e), ranged from 0.6 to 2.2 mmol.L^{-1}, consistent with Guyana's mangroves (Marchand et al., 2006). DOC concentrations were lower at sites furthest from mangroves, with values around 0.2 mmol.L^{-1} at C site.

PCA revealed main drivers of sediment characteristics, accounting for 63% of total variance (Fig. 2C). Stations with higher positive coordinates on axis 1, closer to mangroves, tend to have higher levels of TOC, metals and major elements like K, Ti, Na, P, and Al. Ultramafic sites (C and P) showed negative

positioning on this axis, associated with Ni and Fe. Dumbéa, from a mix of volcanic and ultramafic sources (Fig. 2 and A1), exhibit intermediate values. VKP, characterized by a mix of ultramafic, and volcano-sedimentary (Fig. 2, A1), tend to align positively along this axis, similar to O (metamorphic).

Axis 2 indicated negative values for sand content and positive for clay, silt, and water contents. Stations positioned negatively on this axis, like O-b, O-c, and D-a, had highest sand content and strongest marine influence (Fig. 2c), primarily situated within the bay area (Fig. 1), clearly representing sediment characteristics shaped by marine influences.

3.2. Optical properties of DOM

Table A3 presents a summary of the properties of the porewater sample collected along the Caledonian estuary. Four fluorescent components were validated by PARAFAC analysis using 63 EEMs (Table A4). The four contour plots identified are represented in Fig. 3 with their maximum excitation and emission levels. The spectral characteristics of C1 and C4 components have been identified as humic-like components (Tab. A4), with 2 excitation peaks at 250(330) nm and 270(385) nm and one emission peak at 440 nm and 483 nm for C1 and C4, respectively. The first peak of the C1 component was similar to Humic-like peak A (Coble, 1996) and the second to the humic-like Peak M (Shank et al., 2010). The C2 component has been characterized by two excitation maxima, with peaks at 235 nm and the second at 305 nm with emission around 353-356 nm, which was similar to an autochthonous tryptophane-like component identified as a peak T (Coble et al., 1998). The EEM spectral characteristics of the C3 component were composed of 200 nm excitation maxima and 470-473 nm emission peak. These wavelengths agreed with fulvic-acid (Chen et al., 2003), and UV-humic-like substance (Stedmon et al., 2011).

3.3. Ultramafic geology of the watershed as a driver of DOM

The sites influenced by ultramafic geology share similar characteristics, with low levels of DOM (Table A3). The values of a_{350} range from 7.0 ± 5.2 to 16.2 ± 12.2 m^{-1} in P, from 9.0 ± 8.6 to 22.2 ± 5.9 m^{-1} for C, and from 4.7 ± 1.9 to 17.7 ± 4.3 m^{-1} for VKP. Furthermore, the molecular weights are significantly lower for the four sites with ultramafic catchments. The slope ratio (SR), was greater than 1 for VKP, D, C, and P and < 1 for the O (0.94) site, suggesting high molecular weight terrestrial molecules at O (Fig. 4) (Hansen et al., 2016; Helms et al., 2008). The $S_{275-295}$ and the E_2/E_3 index had the same trend suggested the presence of large and aromatic molecules at D (average value of 1.53 ± 0.57) and small-size molecules with low aromaticity at VKP (average of 3.86 ± 0.83) (Thomsen et al., 2002). Ultramafic geology influences sediment porewater DOM characteristics, including lower levels and molecular weights, as shown by indicators such as SR and E_2/E_3 indices.

Biological activity may contribute to the low CDOM level at VKP, C, and P sites, as suggested by the low a_{350} values. These sites exhibit characteristics of autochthonous DOM activity, similar to the Guayana Shield lagoon impacted by gold mining (Yamashita et al., 2010). Furthermore, Martias et al. (2018) showed CDOM removal by biological processes in the lagoon of New Caledonia, which has a high level of primary productivity compared to other tropical lagoons (Tedetti et al., 2011). The indicators of aromaticity (E2/E3) at VKP suggest significant biological activity with small molecules, possibly from exudation and release of cell contents during normal cell growth cycle (Mayer et al., 1999).

Regardless of the fluorescent compounds identified, P and C sites (most influenced by ultramafic soil) did not exhibit statistically significant differences. The tryptophan-like compound C2, likely derived from heterotrophic bacteria (Coble, 1996), was correlated with biological activity indicators (BIX, E2/E3, S-spectral slopes; Tab.1), suggesting a biological origin, despite Zhao et al. (2017) attributing such compounds to polluted water discharge. The biological index (BIX) was 1.67 ± 0.99 for C and about 1.12 ± 0.44 for VKP (Tab. A3), significantly higher than the D site D (0.88 ± 0.18). The C2 contributions were notably lower at site D, linking C2 to the site's biological activity.

The sediment's nature and metal content might explain the observed biological activity. Low contributions of certain FDOM compounds (C4) could be attributed to a quenching by metals, which inhibit fluorescence (Wang et al., 2017). This could explain the reduced detection of high molecular weight terrestrial molecules at VKP, C, P, and D, supported by the negative correlation between C4 pseudo-concentration and Co (Spearman; p-value < 0.05). Mayer et al. (1999) noted challenges in detecting protein-like molecules due to terrestrial inputs. Further research is needed to understand quenching in metal-rich sediments and its impact on DOM fluorescence. This trend of higher biological activity may also be linked to increased human activities and mining in these areas, as Amaral et al. (2023) found in the anthropized lagoon of Menor in Spain.

3.4. Catchment size and river input as drivers of DOM composition

The average absorption coefficient at 350 nm, a proxy for terrigenous matter in coastal systems, varied from 11.4 ± 5.5 m^{-1} at VKP to 72.7 ± 81.4 m^{-1} at O (Fig.4). VKP, O, and D sites showed a high degree of intra-site variability ($p < 0.05$), more than those of C and P. Statistical analyses revealed two distinct groups among sites: no significant differences between C, P, and VKP, and between D and O. The similarity between O and D sites could be due to their large catchment areas and high river flow rates (Bird et al., 1984; Fernandez et al., 2017). This is supported by Yamashita et al. (2010), who found high terrestrial DOM during the wet season in Venezuela. Although the size of the catchment area had an impact on the characteristics of the DOM, the residence time of the water in the estuary could also be an influencing factor (Battin et al., 2008). Compounds C3 (fulvic acid) and C4 (terrestrial humic-like) showed higher contributions at O and D, and lower at VKP, C, and P. The highest contributions of C4 were at O and D, with O showing significantly higher fulvic acid concentrations than D. Elevated presence of fulvic acid is often associated with an allochthonous origin of dissolved carbon (Hood et al., 2003). The disparity in fulvic-like FDOM contribution between sites can be attributed to more substantial fluvial inputs (O: 4.0 $m^3 . s^{-1}$, D: 3.4 $m^3 . s^{-1}$).

303 The terrestrial origin of these two compounds in our study seems linked to the river water inputs
304 carrying humic matter, consistent with the high CDOM concentrations, high a_{350} and a_{442} values, high
305 molecular weight (SR: 0.94 ± 0.34 for O) and aromaticity (E2/E3: 1.53 ± 0.57 for D).

307 **3.5. Presence of mangrove forests as drivers of DOM**

308 The fluorescent compound C1, characterized as humic-like and identified by both A and M peaks (Table
309 A4), was abundant at the O and VKP sites, and at D for stations (b, c, d), surrounded by mangroves. C1
310 exhibited its highest concentration at the O (22.18 ± 10.83 (A.U) and VKP (16,10 ± 6.78 (A.U). Statistical
311 analysis grouped C1 contributions into O and VKP sites versus D, C, and P sites (Fig. 5). Shank et al.
312 (2010) reported that mangrove-leached material predominantly exhibited similar humic A. Tannins
313 from senescent mangrove leaves were suggested as a source of M-type humic acid (Maie et al., 2008).
314 The presence of C1 in sediment porewater likely comes from mangrove litter, a significant organic
315 carbon reservoir (Alongi, 1997). This hypothesis is supported by the significant negative exponential
316 relationship between the C1 concentration and the distance from the mangrove ($p < 0.01$).

317 TOC and DOC concentrations varied within the same site, ranging from 13.9 ± 0.9 $mg.g^{-1}$ (TOC) and 0.4
318 ± 0.0 $mmol.l^{-1}$ (DOC) at VKP-a to 59.3 ± 2.1 $mg.g^{-1}$ (TOC) and 0.8 ± 0.2 $mmol.l^{-1}$ (DOC) at VKP-c. Similar
319 trend were observed at other sites, including O, with TOC concentrations ranging from 18.7 ± 1.4 $mg.g^{-1}$
320 for O-b to 47.6 ± 2.0 $mg.g^{-1}$ for O-d.

321 This variability supports previous findings of high organic carbon in mangroves of southern New
322 Caledonia (Marchand et al., 2011). The differences in carbon and physico-chemical parameters within
323 sites align with C1 contributions at VKP and O, highlighting the influence of mangrove debris on local
324 conditions (Marchand et al., 2012).

325 Behnke et al. (2023) demonstrated that vegetation freshness influences DOM signals with fresher
326 vegetation retaining more detectable signatures compared to microbially degraded DOM. As DOM
327 undergoes degradation through microbial processes, the signature of DOM sources is progressively

eliminated. Humic sediments help retain detectable signals from these sources (Behnke et al., 2023). Knoke et al. (2024) found that, mangrove-derived DOM retains its recalcitrance even after exportation. Our findings, suggest that the C1 compound may partly originate from mangrove and primary producers.

4. Conclusion

By characterizing the DOM of sediment porewater across estuaries with varying geological influences, we identified four distinct fluorophores. Our findings reveal that porewater DOM comprises both autochthonous (C1, C2) and allochthonous (C3, C4) materials. This study highlights a strong site effect driven by three main factors. Firstly, the geology of the sediments, particularly ultramafic soils and the presence of mining activities, significantly impacts DOM characteristics, evidenced by the low CDOM content and high biological activity. Secondly, the size of the catchment areas and hydrodynamic inputs result in a high abundance of terrestrial humic-like and fulvic-like compounds. Lastly, the presence of mangroves influences the occurrence of humic-like mangrove compounds (C1). Our study provides insights into DOM optical signatures typical of ecosystems like ultramafic sediments or mangroves, valuable for water quality assessment and ecosystem management in estuarine and coastal environments.

5. References

Alongi, D. M. (1997). *Coastal ecosystem processes* (CRC Press).

Amaral, V., Santos-Echeandía, J., Ortega, T., Álvarez-Salgado, X. A., & Forja, J. (2023). Dissolved organic matter distribution in the water column and sediment pore water in a highly anthropized coastal lagoon (Mar Menor, Spain): Characteristics, sources, and benthic fluxes. *Science of The Total Environment*, *896*, 165264. https://doi.org/10.1016/j.scitotenv.2023.165264

Ambatsian, P., Fernex, F., Bernat, M., Parron, C., & Lecolle, J. (1997). High metal inputs to closed seas: The New Caledonian lagoon. *Journal of Geochemical Exploration*, *59*(1), 59–74. https://doi.org/10.1016/S0375-6742(96)00020-9

Baker, A. (2001). Fluorescence excitation - Emission matrix characterization of some sewage-impacted rivers. *Environmental Science and Technology*, *35*(5), 948–953. https://doi.org/10.1021/es000177t

Baker, A. (2002). Fluorescence excitation-emission matrix characterization of river waters impacted by a tissue mill effluent. *Environmental Science and Technology*, *36*(7), 1377–1382. https://doi.org/10.1021/es0101328

Battin, T. J., Kaplan, L. A., Findlay, S., Hopkinson, C. S., Marti, E., Packman, A. I., Newbold, J. D., & Sabater, F. (2008). Biophysical controls on organic carbon fluxes in fluvial networks. *Nature Geoscience*, *1*(2), 95–100. https://doi.org/10.1038/ngeo101

Behnke, M. I., Fellman, J. B., D'Amore, D. V., & Spencer, R. G. M. (2023). Trees in the Stream: Determining Patterns of Terrestrial Dissolved Organic Matter Contributions to the Northeast Pacific Coastal Temperate Rainforest. *Journal of Geophysical Research: Biogeosciences*, *128*(4). https://doi.org/10.1029/2022JG007027

365 [65] Bird, E. C. F., Dubois, J. P., & Iltis, J. A. (1984). *The Impact of Opencast Mining on the Rivers and Coasts of*
366 *New Caledonia*. The United Nation University : Shibuya, Japan.
367 http://archive.unu.edu/unupress/%0Aunupbooks/80505e/80505E00.htm

368 [68] Blair, N. E., & Aller, R. C. (2012). The fate of terrestrial organic carbon in the Marine environment. *Annual*
369 *Review of Marine Science*, *4*, 401–423. https://doi.org/10.1146/annurev-marine-120709-142717

370 [70] Bourgeois, C., Alfaro, A. C., Bisson, E., Alcius, S., & Marchand, C. (2020). Trace metal dynamics in soils and
371 plants along intertidal gradients in semi-arid mangroves (New Caledonia). *Marine Pollution Bulletin*,
372 *156*. https://doi.org/10.1016/j.marpolbul.2020.111274

373 [73] Burdige, D. J. (2001). Dissolved organic matter in Chesapeake Bay sediment pore waters. *Organic*
374 *Geochemistry*, *32*(4), 487–505. https://doi.org/10.1016/S0146-6380(00)00191-1

375 [75] Burdige, D. J., Kline, S. W., & Chen, W. (2004). Fluorescent dissolved organic matter in marine sediment
376 pore waters. *Marine Chemistry*, *89*(1–4), 289–311. https://doi.org/10.1016/j.marchem.2004.02.015

377 [77] Cai, W. J. (2011). Estuarine and coastal ocean carbon paradox: CO 2 sinks or sites of terrestrial carbon
378 incineration? *Annual Review of Marine Science*, *3*, 123–145. https://doi.org/10.1146/annurev-
379 marine-120709-142723

380 [80] Chen, M., & Hur, J. (2015). Pre-treatments, characteristics, and biogeochemical dynamics of dissolved
381 organic matter in sediments: A review. *Water Research*, *79*, 10–25.
382 https://doi.org/10.1016/j.watres.2015.04.018

383 [83] Chen, W., Westerhoff, P., Leenheer, J. A., & Booksh, K. (2003). Fluorescence Excitation-Emission Matrix
384 Regional Integration to Quantify Spectra for Dissolved Organic Matter. *Environmental Science and*
385 *Technology*, *37*(24), 5701–5710. https://doi.org/10.1021/es034354c

386 [86] Coble, P. G. (1996). Characterization of marine and terrestrial DOM in seawater using excitation-emission
387 matrix spectroscopy. *Marine Chemistry*, *51*(4), 325–346. https://doi.org/10.1016/0304-
388 4203(95)00062-3

389 [89] Coble, P. G., Castillo, C. E. Del, & Avril, B. (1998). Distribution and optical properties of CDOM in the
390 Arabian Sea during the 1995 Southwest Monsoon. In *Deep-Sea Research II* (Vol. 45).

391 [91] Desclaux, T., Lemonnier, H., Genthon, P., Soulard, B., & Le Gendre, R. (2018). Suitability of a lumped
392 rainfall–runoff model for flashy tropical watersheds in New Caledonia. *Hydrological Sciences Journal*,
393 *63*(11), 1689–1706. https://doi.org/10.1080/02626667.2018.1523613

394 [94] Dittmar, T., & Lara, R. J. (2001). Driving forces behind nutrient and organic matter dynamics in a mangrove
395 tidal creek in North Brazil. *Estuarine, Coastal and Shelf Science*, *52*(2), 249–259.
396 https://doi.org/10.1006/ecss.2000.0743

397 [97] Dublet, G., Juillot, F., Morin, G., Fritsch, E., Fandeur, D., & Brown, G. E. (2015). Goethite aging explains Ni
398 depletion in upper units of ultramafic lateritic ores from New Caledonia. *Geochimica et*
399 *Cosmochimica Acta*, *160*, 1–15. https://doi.org/10.1016/j.gca.2015.03.015

400 [100] Dubuc, A., Rummer, J. L., Vigliola, L., & Lemonnier, H. (2024). Coping with environmental degradation:
401 Physiological and morphological adjustments of wild mangrove fish to decades of aquaculture-
402 induced nutrient enrichment. *Marine Pollution Bulletin*, *205*.
403 https://doi.org/10.1016/j.marpolbul.2024.116599

[4] Fernandez, J. M., Meunier, J. D., Ouillon, S., Moreton, B., Douillet, P., & Grauby, O. (2017). Dynamics of suspended sediments during a dry season and their consequences on metal transportation in a Coral reef lagoon impacted by mining activities, New Caledonia. *Water (Switzerland)*, *9*(5). https://doi.org/10.3390/w9050338

[8] Fichez, R., Chifflet, S., Douillet, P., Gérard, P., Gutierrez, F., Jouon, A., Ouillon, S., & Grenz, C. (2010). Biogeochemical typology and temporal variability of lagoon waters in a coral reef ecosystem subject to terrigeneous and anthropogenic inputs (New Caledonia). *Marine Pollution Bulletin*, *61*(7–12), 309–322. https://doi.org/10.1016/j.marpolbul.2010.06.021

[12] Hansen, A. M., Kraus, T. E. C., Pellerin, B. A., Fleck, J. A., Downing, B. D., & Bergamaschi, B. A. (2016). Optical properties of dissolved organic matter (DOM): Effects of biological and photolytic degradation. *Limnology and Oceanography*, *61*(3), 1015–1032. https://doi.org/10.1002/lno.10270

[15] He, Y., Men, B., Yang, X., Li, Y., Xu, H., & Wang, D. (2019). Relationship between heavy metals and dissolved organic matter released from sediment by bioturbation/bioirrigation. *Journal of Environmental Sciences (China)*, *75*, 216–223. https://doi.org/10.1016/j.jes.2018.03.031

[18] Helms, J., Stubbins, A., Ritchie, J. D., Minor, E. C., Kieber, D. J., & Mopper, K. (2008). Absorption spectral slopes and slope ratios as indicators of molecular weight, source, and photobleaching of chromophoric dissolved organic matter (Limnology and Oceanography 53 955-969). *Limnology and Oceanography*, *54*(3), 1023. https://doi.org/10.4319/lo.2009.54.3.1023

[22] Hood, E., McKnight, D. M., & Williams, M. W. (2003). Sources and chemical character of dissolved organic carbon across an alpine/subalpine ecotone, Green Lakes Valley, Colorado Front Range, United States. *Water Resources Research*, *39*(7), 1–12. https://doi.org/10.1029/2002WR001738

[25] Jaffé, R., Boyer, J. N., Lu, X., Maie, N., Yang, C., Scully, N. M., & Mock, S. (2004). Source characterization of dissolved organic matter in a subtropical mangrove-dominated estuary by fluorescence analysis. *Marine Chemistry*, *84*(3–4), 195–210. https://doi.org/10.1016/j.marchem.2003.08.001

[28] Kierczak, J., Pietranik, A., & Pędziwiatr, A. (2021). Ultramafic geoecosystems as a natural source of Ni, Cr, and Co to the environment: A review. In *Science of the Total Environment* (Vol. 755). Elsevier B.V. https://doi.org/10.1016/j.scitotenv.2020.142620

[31] Knoke, M., Dittmar, T., Zielinski, O., Kida, M., Asp, N. E., de Rezende, C. E., Schnetger, B., & Seidel, M. (2024). Outwelling of reduced porewater drives the biogeochemistry of dissolved organic matter and trace metals in a major mangrove-fringed estuary in Amazonia. *Limnology and Oceanography*, *69*(2), 262–278. https://doi.org/10.1002/lno.12473

[35] Lulau, N., Soulard, B., & Le Gendre, R. (2019). *Atlas 2011-2017 des apports hydriques à l'échelle du territoire calédonien Projet Présence*.

[37] Paulie, A. R., & Brothers, R. N. (1970). The geology of New Caledonia. *New Zealand Journal of Geology and Geophysics*, *13*(1), 145–183. https://doi.org/10.1080/00288306.1970.10428210

[39] Maie, N., Pisani, O., & Jaffé, R. (2008). Mangrove tannins in aquatic ecosystems: Their fate and possible influence on dissolved organic carbon and nitrogen cycling. *Limnology and Oceanography*, *53*(1), 160–171. https://doi.org/10.4319/lo.2008.53.1.0160

Marchand, C., Albéric, P., Lallier-Vergès, E., & Baltzer, F. (2006). Distribution and characteristics of dissolved organic matter in mangrove sediment pore waters along the coastline of French Guiana. *Biogeochemistry*, *81*(1), 59–75. https://doi.org/10.1007/s10533-006-9030-x

Marchand, C., Allenbach, M., & Lallier-Vergès, E. (2011). Relationships between heavy metals distribution and organic matter cycling in mangrove sediments (Conception Bay, New Caledonia). *Geoderma*, *160*(3–4), 444–456. https://doi.org/10.1016/j.geoderma.2010.10.015

Marchand, C., Fernandez, J. M., Moreton, B., Landi, L., Lallier-Vergès, E., & Baltzer, F. (2012). The partitioning of transitional metals (Fe, Mn, Ni, Cr) in mangrove sediments downstream of a ferralitized ultramafic watershed (New Caledonia). *Chemical Geology*, *300–301*, 70–80. https://doi.org/10.1016/j.chemgeo.2012.01.018

Martias, C., Tedetti, M., Lantoine, F., Jamet, L., & Dupouy, C. (2018). Characterization and sources of colored dissolved organic matter in a coral reef ecosystem subject to ultramafic erosion pressure (New Caledonia, Southwest Pacific). *Science of the Total Environment*, *616–617*, 438–452. https://doi.org/10.1016/j.scitotenv.2017.10.261

Maurizot, P., Robineau, B., Vendé-Leclerc, M., & Cluzel, D. (2020). Introduction to New Caledonia: Geology, geodynamic evolution and mineral resources. In *Geological Society Memoir* (Vol. 51, Issue 1, pp. 1–12). Geological Society of London. https://doi.org/10.6084/m9.figshare.c.4984385

Mayer, L. M., Schick, L. L., & Loder, T. C. (1999). Dissolved protein fluorescence in two maine estuaries. *Marine Chemistry*, *64*(3), 171–179. https://doi.org/10.1016/S0304-4203(98)00072-3

McKnight, D. M., Boyer, E. W., Westerhoff, P. K., Doran, P. T., Kulbe, T., & Andersen, D. T. (2001). Spectrofluorometric characterization of dissolved organic matter for indication of precursor organic material and aromaticity. *Limnology and Oceanography*, *46*(1), 38–48. https://doi.org/10.4319/lo.2001.46.1.0038

Mounier, S., Zhao, H., Garnier, C., & Redon, R. (2011). Copper complexing properties of dissolved organic matter: PARAFAC treatment of fluorescence quenching. *Biogeochemistry*, *106*(1), 107–116. https://doi.org/10.1007/s10533-010-9486-6

National Oceanic and Atmospheric Administration (NOAA) Oceanic Niño Index (ONI) v5. (2023, January 9). https://origin.cpc.ncep.noaa.gov/products/analysis_monitoring/ensostuff/ONI_v5.php

Nelson, N. B., & Siegel, D. A. (2013). The global distribution and dynamics of chromophoric dissolved organic matter. *Annual Review of Marine Science*, *5*, 447–476. https://doi.org/10.1146/annurev-marine-120710-100751

Parlanti, E., Wörz, K., Geoffroy, L., & Lamotte, M. (2000). Dissolved organic matter fluorescence spectroscopy as a tool to estimate biological activity in a coastal zone submitted to anthropogenic inputs. *Organic Geochemistry*, *31*(12), 1765–1781. https://doi.org/10.1016/S0146-6380(00)00124-8

Payri, C. E., Allain, V., Aucan, J., David, C., David, V., Dutheil, C., Loubersac, L., Menkes, C., Pelletier, B., Pestana, G., & Samadi, S. (2018). New Caledonia. In *World Seas: An Environmental Evaluation Volume II: The Indian Ocean to the Pacific* (pp. 593–618). Elsevier. https://doi.org/10.1016/B978-0-08-100853-9.00035-X

480 [80] Robin, S. L., Marchand, C., Mathian, M., Baudin, F., & Alfaro, A. C. (2022). Partitioning and Bioaccumulation
481 of Trace Metals in Urban Mangrove Ecosystems (New Caledonia). *SSRN Electronic Journal*.
482 https://doi.org/10.2139/ssrn.4103353

483 [83] Santos, I. R., Burdige, D. J., Jennerjahn, T. C., Bouillon, S., Cabral, A., Serrano, O., Wernberg, T., Filbee-
484 Dexter, K., Guimond, J. A., & Tamborski, J. J. (2021). The renaissance of Odum's outwelling hypothesis
485 in "Blue Carbon" science. *Estuarine, Coastal and Shelf Science*, *255*.
486 https://doi.org/10.1016/j.ecss.2021.107361

487 [87] Shank, G. C., Lee, R., Vähätalo, A., Zepp, R. G., & Bartels, E. (2010). Production of chromophoric dissolved
488 organic matter from mangrove leaf litter and floating Sargassum colonies. *Marine Chemistry*, *119*(1–
489 4), 172–181. https://doi.org/10.1016/j.marchem.2010.02.002

490 [90] Stedmon, C. A., Thomas, D. N., Papadimitriou, S., Granskog, M. A., & Dieckmann, G. S. (2011). Using
491 fluorescence to characterize dissolved organic matter in Antarctic sea ice brines. *Journal of*
492 *Geophysical Research: Biogeosciences*, *116*(3). https://doi.org/10.1029/2011JG001716

493 [92] Tedetti, M., Cuet, P., Guigue, C., & Goutx, M. (2011). Characterization of dissolved organic matter in a coral
494 reef ecosystem subjected to anthropogenic pressures (La Réunion Island, Indian Ocean) using multi-
495 dimensional fluorescence spectroscopy. *Science of the Total Environment*, *409*(11), 2198–2210.
496 https://doi.org/10.1016/j.scitotenv.2011.01.058

497 [97] Thomsen, M., Dobel, S., Lassen, P., Carlsen, L., Mogensen, B. B., & Hansen, P. E. (2002). Reverse
498 quantitative structure-activity relationship for modelling the sorption of esfenvalerate to dissolved
499 organic matter: A multivariate approach. *Chemosphere*, *49*(10), 1317–1325.
500 https://doi.org/10.1016/S0045-6535(02)00510-6

501 [101] Walkley, M. G., Swenson, L. J., Patterson, D. D., & Dahnke, W. C. (1992). Organic Carbon Determination by
502 the Walkley-Black, Udy Dye, and Dry Combustion Methods for Selected North Dakota Soils.
503 *Communications in Soil Science and Plant Analysis*, *23*(3–4), 417–429.
504 https://doi.org/10.1080/00103629209368599

505 [105] Vincent, D. G. (1994). The South Pacific Convergence Zone (SPCZ): A Review. *Monthly Weather Review*,
506 *122*. https://doi.org/https://doi.org/10.1175/1520-0493(1994)122<1949:TSPCZA>2.0.CO;2

507 [107] Wang, L., Li, H., Yang, Y., Zhang, D., Wu, M., Pan, B., & Xing, B. (2017). Identifying structural characteristics
508 of humic acid to static and dynamic fluorescence quenching of phenanthrene, 9-phenanthrol, and
509 naphthalene. *Water Research*, *122*, 337–344. https://doi.org/10.1016/j.watres.2017.06.010

510 [110] Wu, J., Zhang, H., He, P. J., & Shao, L. M. (2011). Insight into the heavy metal binding potential of dissolved
511 organic matter in MSW leachate using EEM quenching combined with PARAFAC analysis. *Water*
512 *Research*, *45*(4), 1711–1719. https://doi.org/10.1016/j.watres.2010.11.022

513 [113] Wu, S., Tao, S., Ye, X., Wang, A., Liu, Z., Ran, C., Liang, H., Li, H., Yang, Y., Zhang, W., & Liu, J. T. (2023).
514 Characteristics of Sedimentary Organic Matter in Tidal Estuaries: A Case Study from the Minjiang
515 River Estuary. *Water (Switzerland)*, *15*(9). https://doi.org/10.3390/w15091682

516 [116] Yamashita, Y., Maie, N., Briceño, H., & Jaffé, R. (2010). Optical characterization of dissolved organic matter
517 in tropical rivers of the Guayana Shield, Venezuela. *Journal of Geophysical Research: Biogeosciences*,
518 *115*(G1). https://doi.org/10.1029/2009JG000987

Zepp, R. G., Sheldon, W. M., & Moran, M. A. (2004). Dissolved organic fluorophores in southeastern US coastal waters: Correction method for eliminating Rayleigh and Raman scattering peaks in excitation-emission matrices. *Marine Chemistry*, *89*(1–4), 15–36. https://doi.org/10.1016/j.marchem.2004.02.006

Zhao, Y., Song, K., Wen, Z., Fang, C., Shang, Y., & Lv, L. (2017). Evaluation of CDOM sources and their links with water quality in the lakes of Northeast China using fluorescence spectroscopy. *Journal of Hydrology*, *550*, 80–91. https://doi.org/10.1016/j.jhydrol.2017.04.027

Zhou, C., Liu, Y., Liu, C., Liu, Y., & Tfaily, M. M. (2019). Compositional changes of dissolved organic carbon during its dynamic desorption from hyporheic zone sediments. *Science of the Total Environment*, *658*, 16–23. https://doi.org/10.1016/j.scitotenv.2018.12

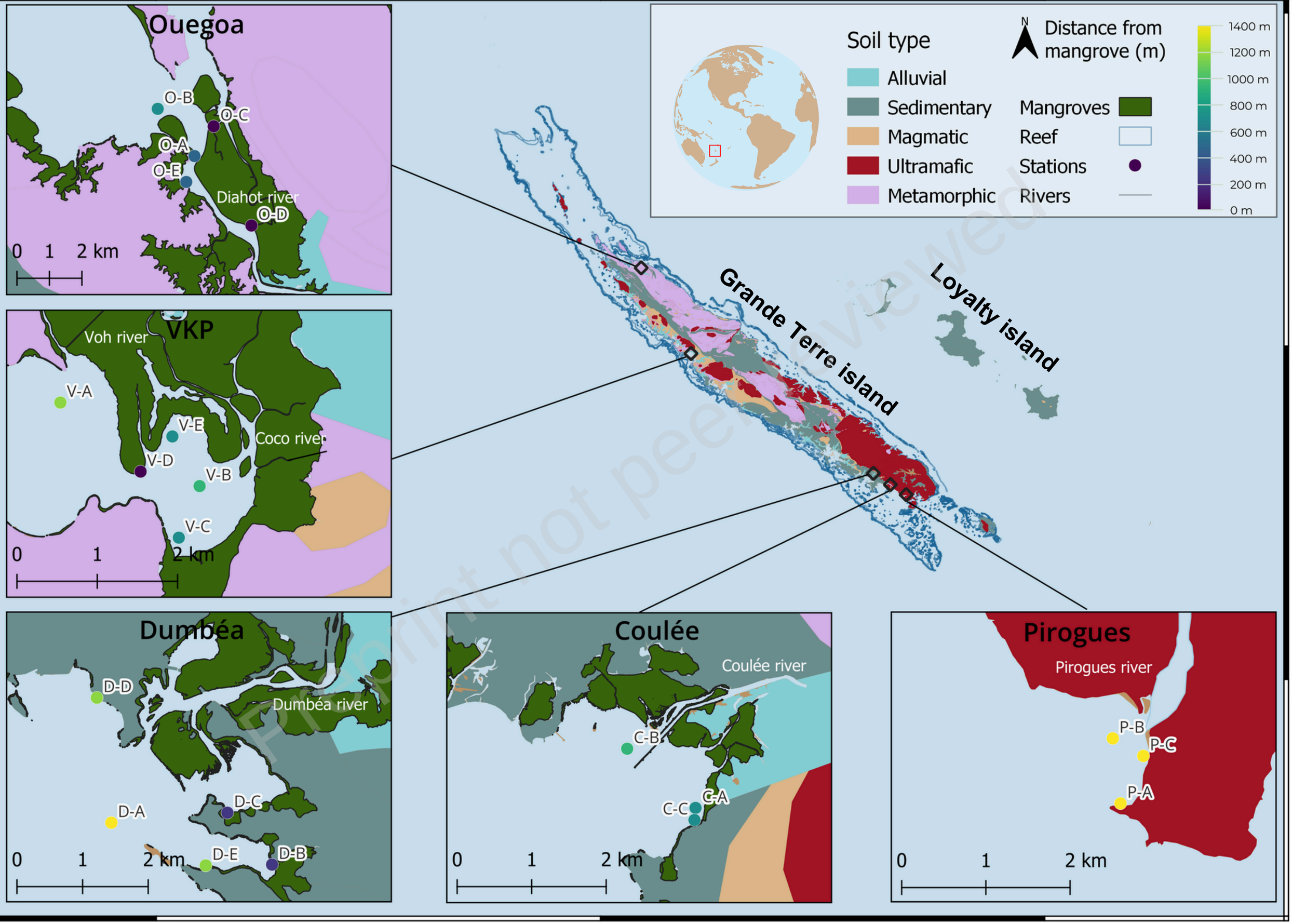

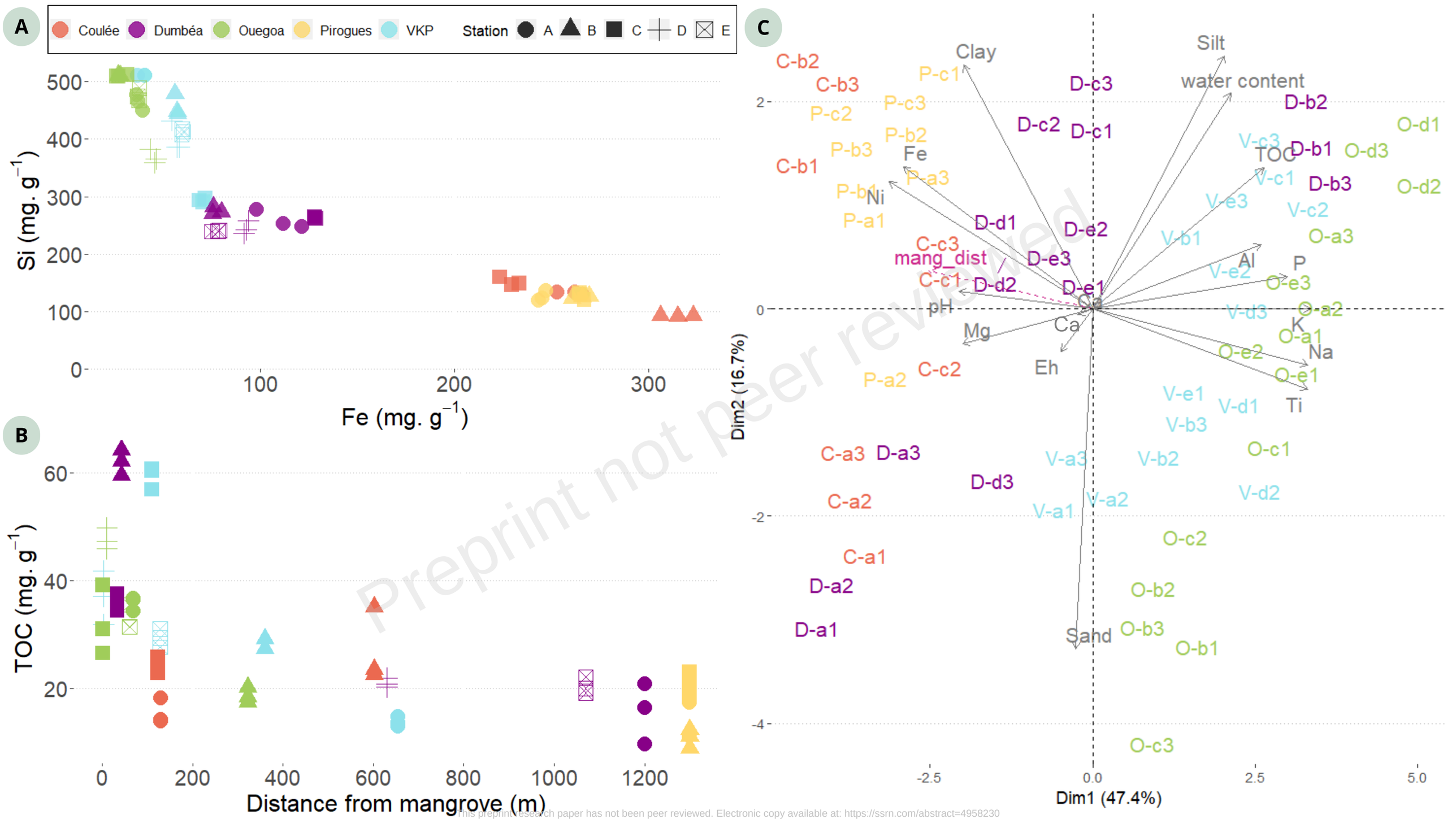

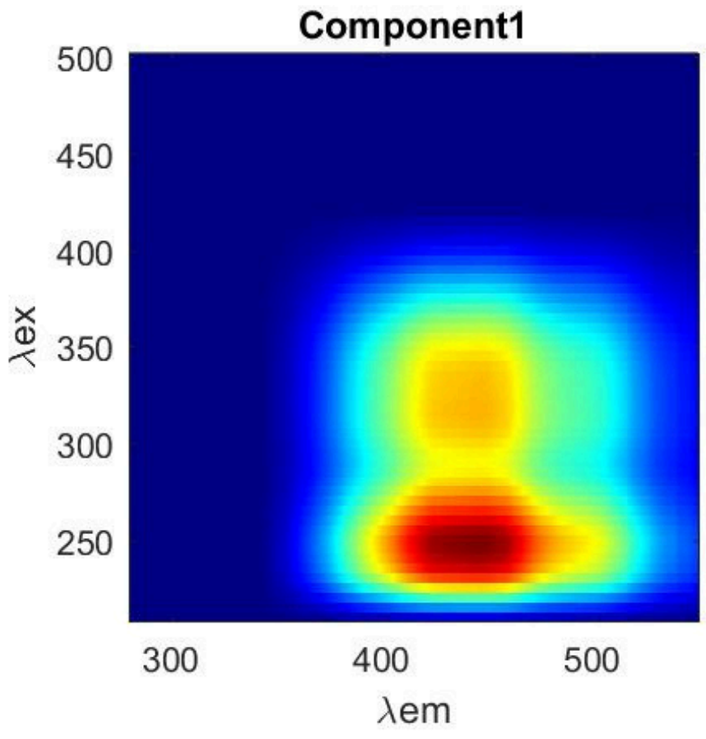

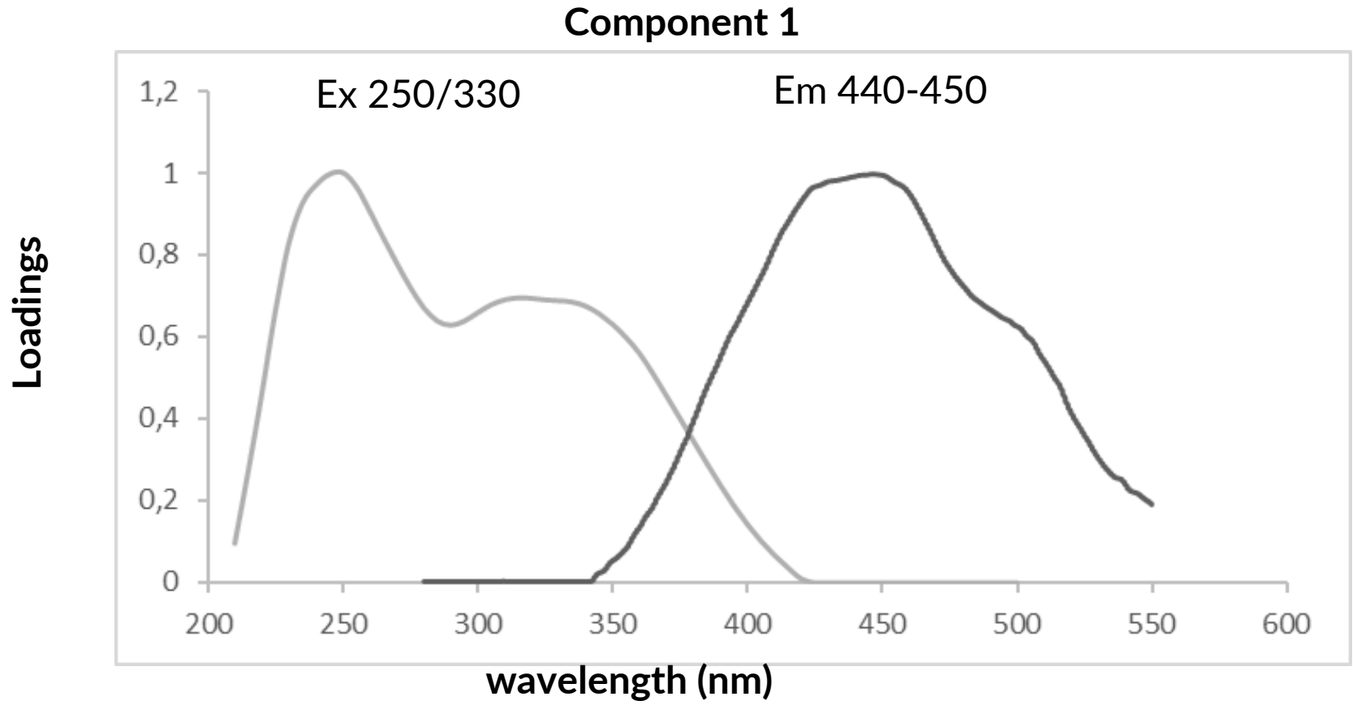

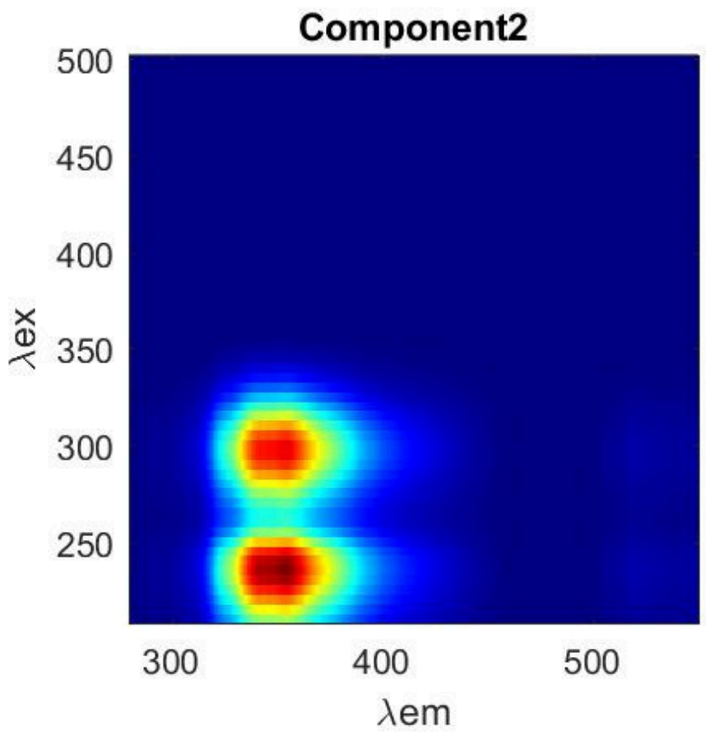

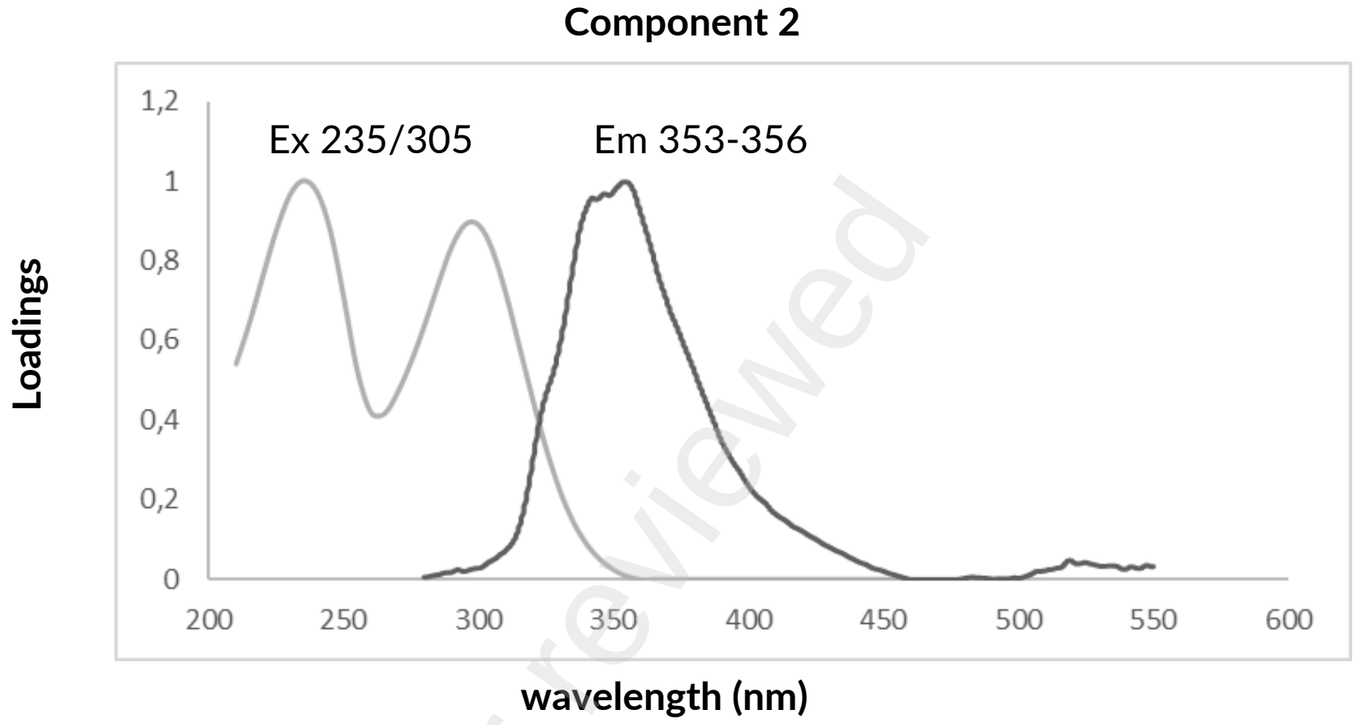

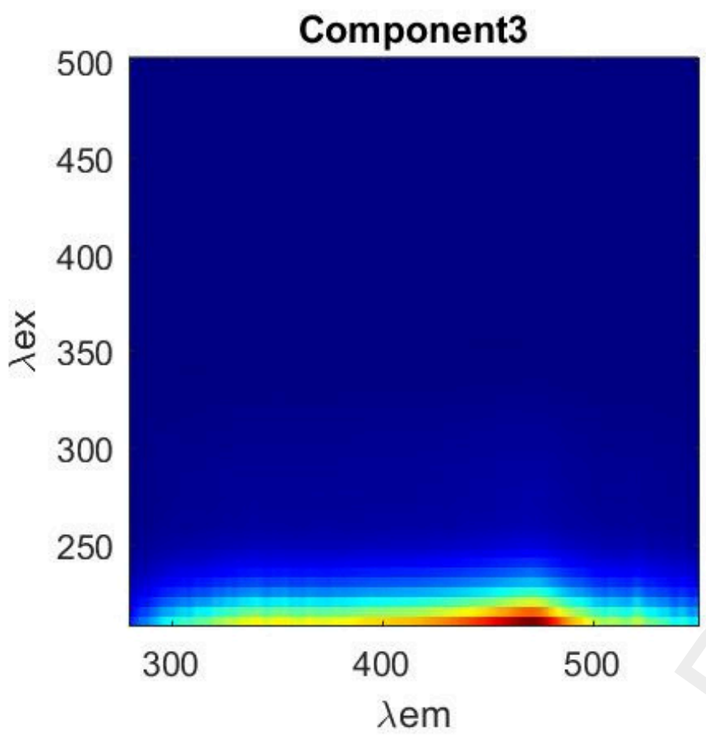

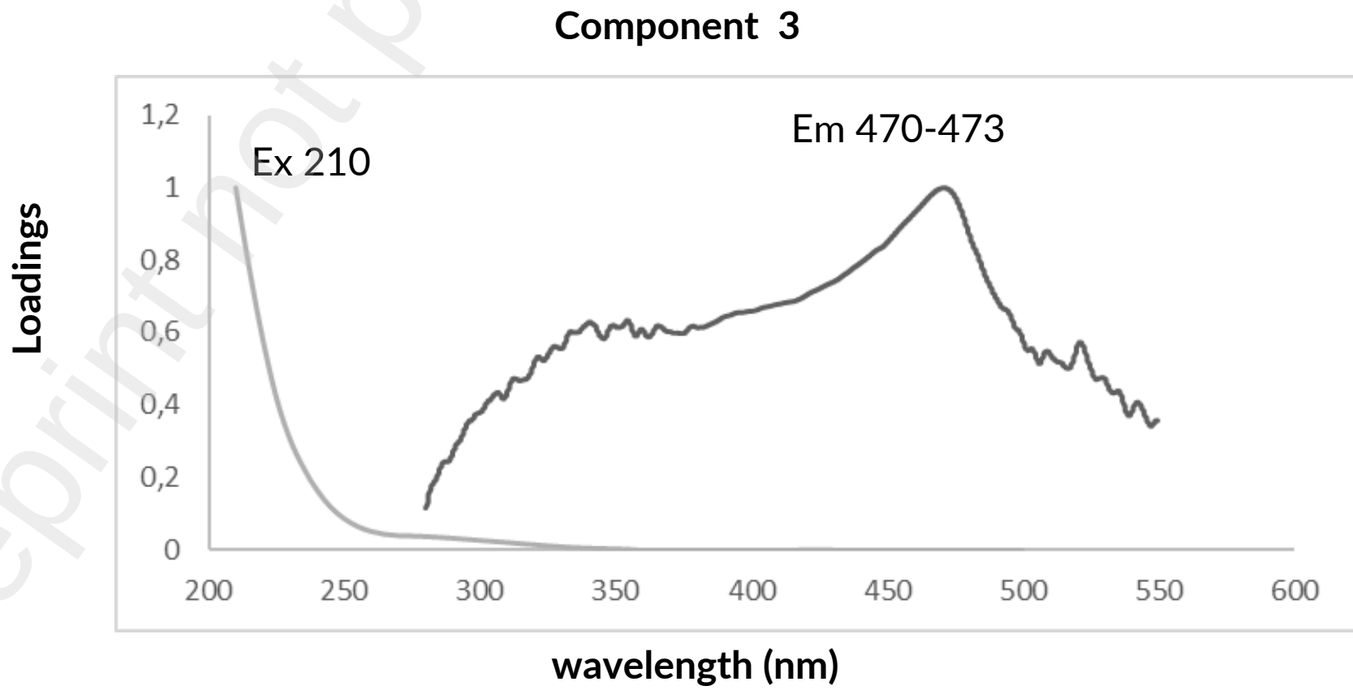

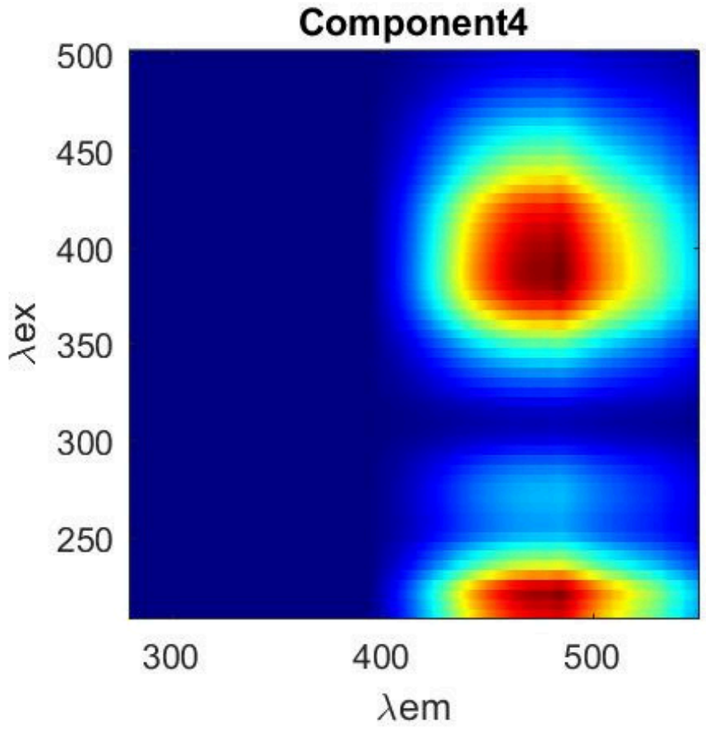

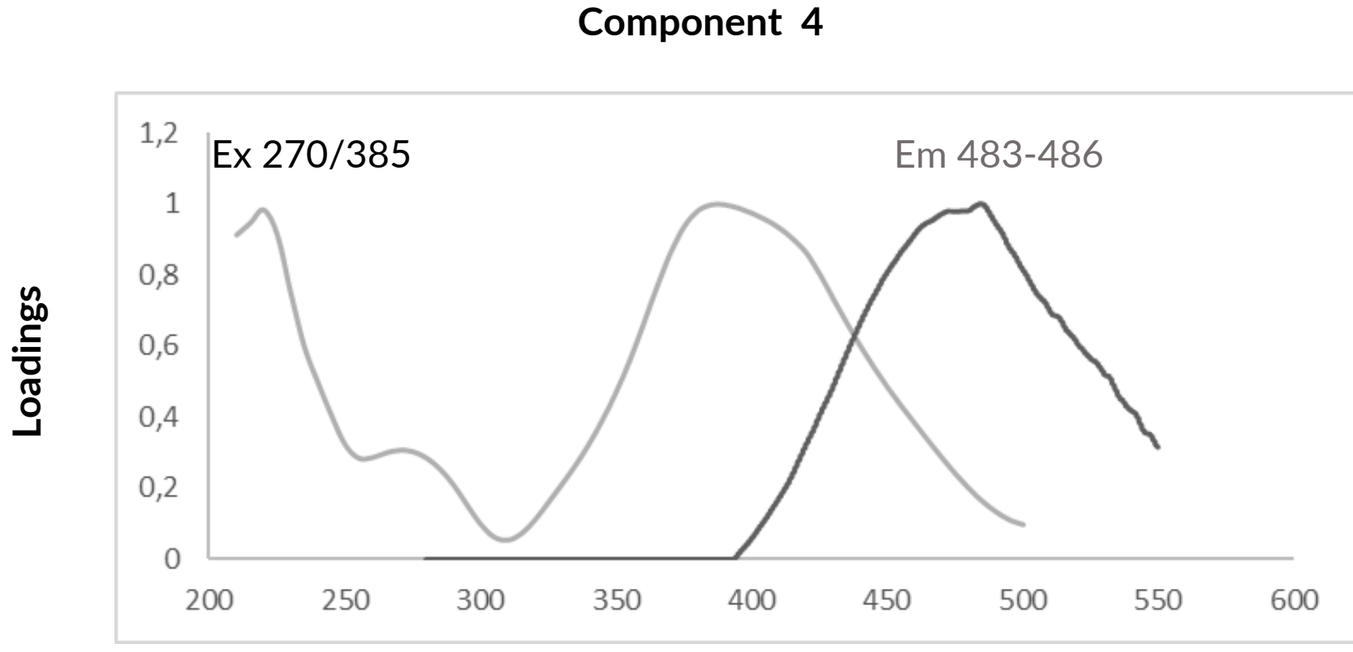

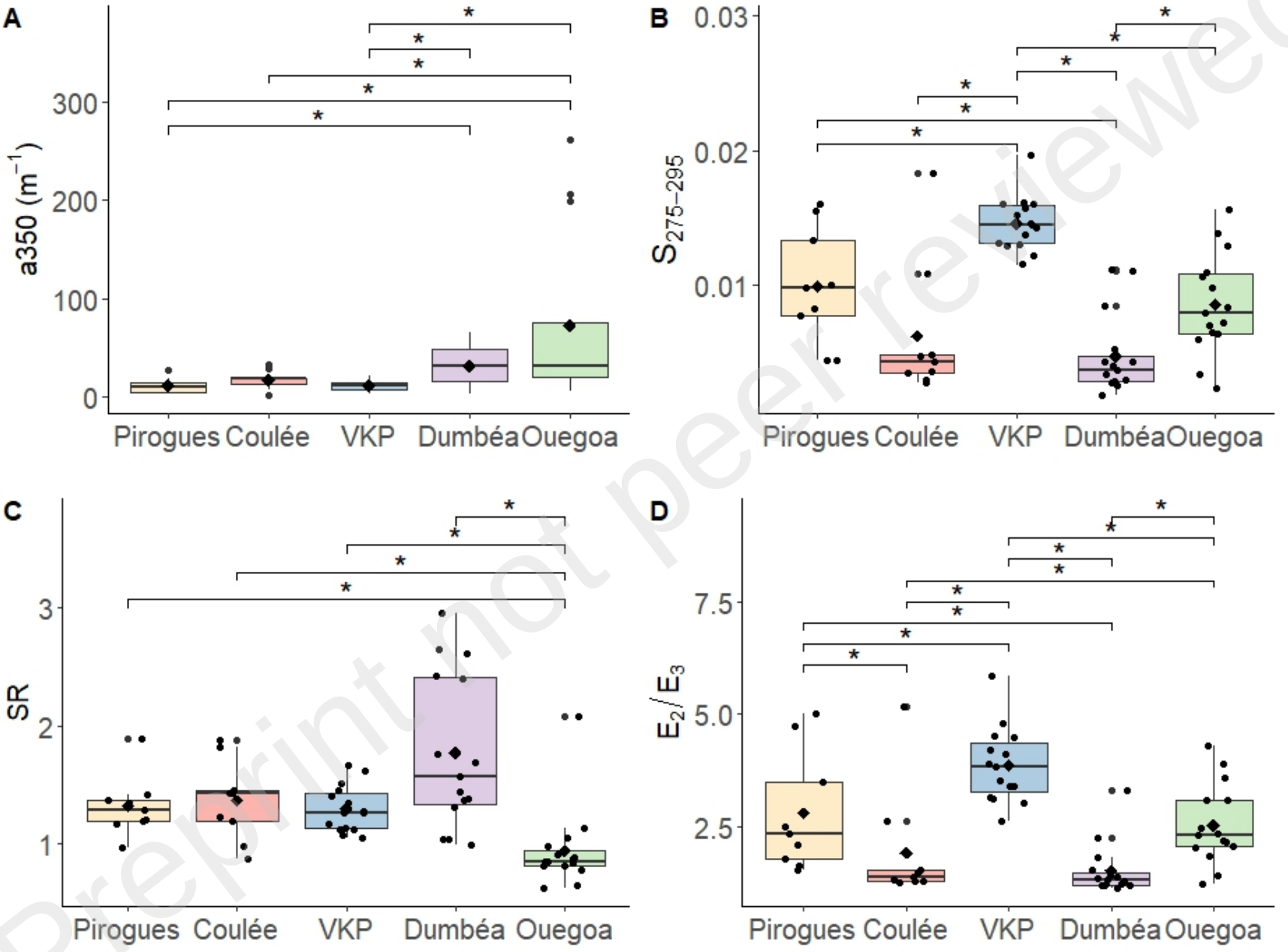

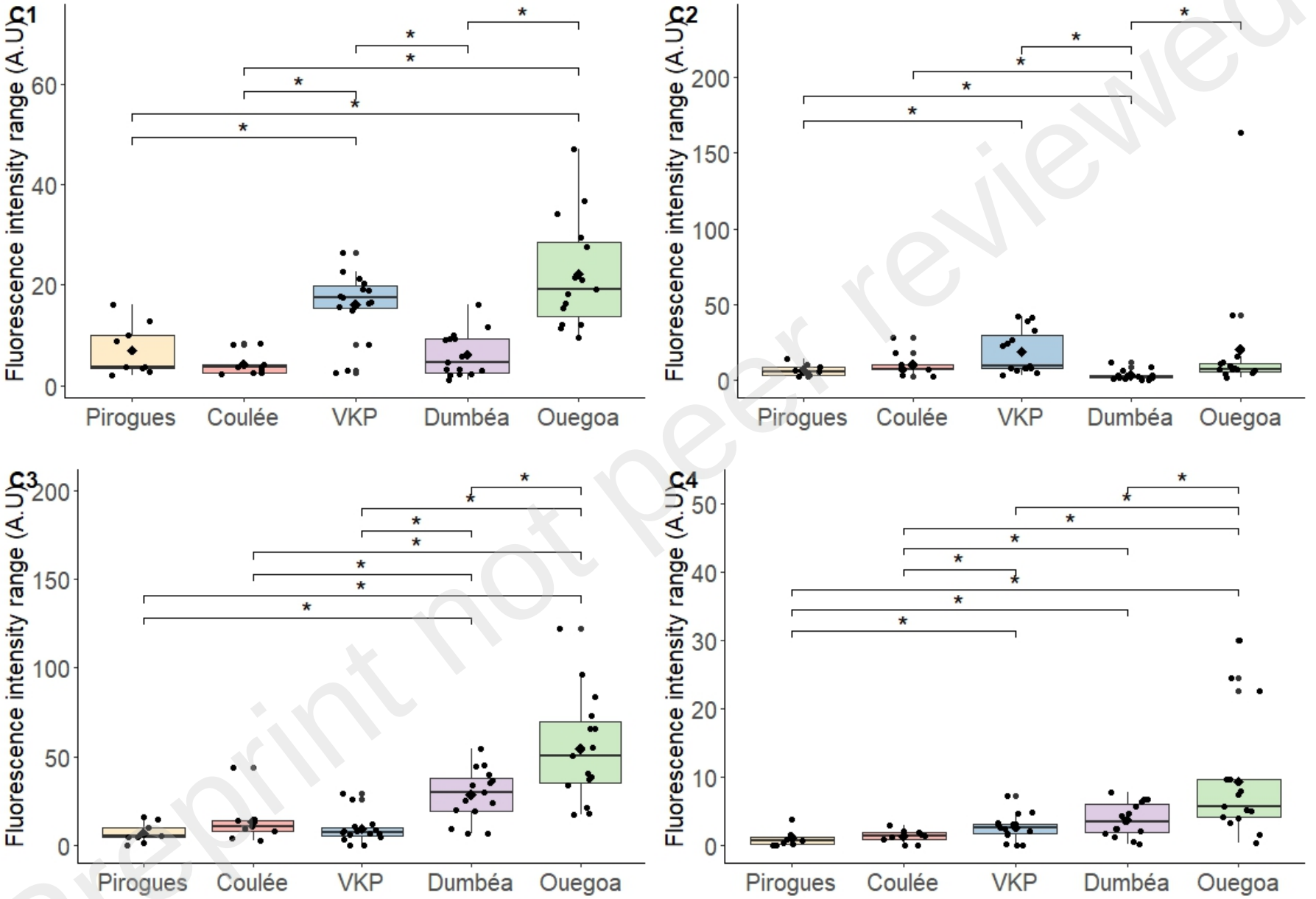

Figures Legends

Figure 1: Map of the five sampling sites. For each site, the 3-5 stations are coded, the first letter corresponds to the site (O for Ouegoa area, V for VKP (Voh-Koné-Pouembout) area, D for Dumbéa and C for Coulée and P for Pirogues) and the second letter refers to the station (a, b, c, d or e). All sites are under varying degrees of ultramafic influence except Ouegoa, and varying distances from mangroves. The map was produced using QGIS (October 2023 based on a 1:50,000 geological map from the Government of New Caledonia / D.I.T.T.T.).

Figure 2: Geological and environmental characterization of sampling sites. A: Station dispersion as related to silica and iron concentrations. B. TOC concentration as a function of distance from mangroves. C: Principal component analysis (PCA) of environmental parameters with the distance to the mangrove as a supplementary variable. Stations are represented by colour codes (orange for Coulée C, purple for Dumbéa D, green for Ouegoa O, yellow for Pirogues P, and blue for VKP). The first letter corresponds to the site, the second letter to the station (from a to e), and the number indicates the replicate (1 to 3).

Figure 3: Spectral characteristics of the four fluorophores approved by the PARAFAC model for samples from 5 sites (Pirogues, Coulée, VKP, Ouegoa, Dumbéa. In the left column, the plot contours, and in the right column, the excitation (grey) and emission (black) spectra.

*Figure 4: CDOM absorption coefficients at 350 nm (m-1) (A), spectral slope S275-295 (B), SR slope ration (C) and E2/E3 ratio (D) for each site (Pirogue: yellow, red: Coulée, VKP: blue, Dumbéa: purple, Ouégoa: green). The mean value is indicated by a black diamond, and the median by a black bar. Significant differences are indicated by stars *: p-value < 0.05. Note that the ordinate axes are not the same between parameters.*

Figure 5: Box plots of DOM fluorescence of four components validated by PARAFAC (C1–C4) in four sites. The mean value is indicated by a black diamond, and the median by a black bar. The fluorophore C1 (Humic-like), the tryptophan-like (C2), the fulvic-acid (C3), and the terrestrial humic-like (C4). Note that the ordinate axes are not the same between fluorophores.

Site	Station	Coordinates		Date	Hour	Salinity	°C
		Long.	Lat.				
VKP	V-a	164°40’42.61"E	20°59’27.81"S	03/09	06:30	33.9	30.6
	V-b	164°41’42.66"E	21° 0’1.43"S	03/09	08:40	33.6	31
	V-c	164°41’33.71"E	21° 0’22.19"S	03/10	10:20	34	31.2
	V-d	164°41’17.21"E	20°59’55.60"S	03/10	07:15	29.6	30.5
	V-e	164°41’30.94"E	20°59’41.45"S	03/10	09:07	19	31.7
Ouegoa	O-a	164°18’5.77"E	20°17’14.65"S	03/16	10:05	29	29.6
	O-b	164°17’26.85"E	20°16’27.97"S	03/16	11:40	31.7	30.5
	O-c	164°18’26.34"E	20°16’45.22"S	03/16	13:30	27.7	30.7
	O-d	164°19’6.33"E	20°18’23.79"S	03/17	09:37	25.9	29.5
	O-e	164°17’57.09"E	20°17’40.32"S	03/17	11:59	24.5	30.2
Dumbéa	D-a	166°24’58.53"E	22°11’39.51"S	03/23	07:00	34.4	28.7
	D-b	166°26’7.68"E	22°12’0.30"S	03/23	08:26	32.5	29.2
	D-c	166°25’43.43"E	22°11’34.47"S	03/23	10:05	32.2	28.9
	D-d	166°24’34.25"E	22°10’38.06"S	03/24	07:27	33.1	28.5
	D-e	166°25’31.94"E	22°12’0.41"S	03/24	09:47	33.5	28.6
Coulée	C-a	166°33’50.57"E	22°15’1.20"S	04/12	10:56	15	26
	C-b	166°33’18.53"E	22°14’35.52"S	04/12	13:05	31	28.5
	C-c	166°33’50.04"E	22°15’6.48"S	04/12	14:24	28.4	27.7
Pirogue	P-a	166°40’51.17"E	22°19’5.97"S	04/13	10:03	22	26.5
	P-b	166°40’47.98"E	22°18’41.00"S	04/13	12:07	34	28.9
	P-c	166°41’0.66"E	22°18’47.74"S	04/13	13:43	22.2	29

Site	Station	Al (mg.g^{-1})	Ca (mg.g^{-1})	Co (µg.g^{-1})	Cr (mg.g^{-1})	Fe (mg.g^{-1})	K (mg.g^{-1})	Ni (mg.g^{-1})	P (µg.g^{-1})	Si (mg.g^{-1})
Pirogues	A	53,0 ± 1,2	22,8 ± 2,9	456 ± 14	22,4 ± 4,1	246 ± 2	0,8 ± 0,1	4,2 ± 0,4	161 ± 8	126 ± 8
	B	56,2 ± 1,3	7,9 ± 1,0	546 ± 15	22,4 ± 1,2	265 ± 4	0,6 ± 0	5,2 ± 0,1	80 ± 8	125 ± 2
	C	55,3 ± 0,5	6,4 ± 0,1	472 ± 9	15,5 ± 0,9	265 ± 1	0,8 ± 0	5,5 ± 0,4	85 ± 3	128 ± 5
Coulée	A	38,0 ± 0,7	20,5 ± 3,2	560 ± 12	17,8 ± 1,2	260 ± 7	1,2 ± 0,1	5,1 ± 0,2	256 ± 7	132 ± 2
	B	39,1 ± 1,0	4,6 ± 0,1	673 ± 18	19 ± 0,6	315 ± 9	0,9 ± 0,1	6,5 ± 0,2	114 ± 10	94 ± 1
	C	39,2 ± 0,4	27,5 ± 1,5	454 ± 11	20,1 ± 0,5	229 ± 5	2,1 ± 0,1	4,4 ± 0,1	317 ± 24	152 ± 7
Dumbéa	A	22,5 ± 3,8	12,8 ± 2,9	217 ± 15	11,4 ± 2,7	110 ± 12	2,1 ± 0,6	3,1 ± 0,2	194 ± 52	259 ± 17
	B	56,0 ± 0,6	17,2 ± 1,2	80 ± 3	2,5 ± 0	77,4 ± 2	8,9 ± 0,1	0,7 ± 0,1	578 ± 10	275 ± 7
	C	37,2 ± 0,5	15,1 ± 0,5	205 ± 3	7,3 ± 0,3	128 ± 1	5,1 ± 0,1	3 ± 0,2	404 ± 32	263 ± 1
	D	34,3 ± 1,2	62,1 ± 11,4	170 ± 2	8,9 ± 0,7	92,9 ± 1,7	4,8 ± 0,2	2,2 ± 0,1	358 ± 23	245 ± 11
	E	38,5 ± 1,4	86,6 ± 10,4	112 ± 4	4,4 ± 0,4	77,9 ± 2,1	7,2 ± 0,2	1,4 ± 0,1	500 ± 48	241 ± 1
VKP	A	47,4 ± 2,5	19,1 ± 1,1	49 ± 2	1,5 ± 0,3	39 ± 2	5,6 ± 0,2	0,5 ± 0	312 ± 55	510 ± 0
	B	56,0 ± 1,8	18,6 ± 0,6	73 ± 0	2 ± 0,4	57 ± 1	7,4 ± 0,2	1 ± 0	442 ± 19	457 ± 18
	C	56,1 ± 0,6	30,8 ±1,7	81 ± 6	1,4 ± 0	70 ± 1	8,5 ± 0,1	1 ± 0,4	536 ± 17	294 ± 4
	D	59,1 ± 1,4	22,4 ± 1,9	66 ± 2	3,1 ± 1,3	56 ± 2	6,8 ± 0,4	0,7 ± 0,2	487 ± 20	402 ± 27
	E	58,5 ± 0,6	18,8 ± 0,8	78 ± 3	1,9 ± 0,1	60 ± 0	7,4 ± 0,1	0,9 ± 0,2	474 ± 11	413 ± 5
Ouegoa	A	69,2 ± 2,0	7,9 ± 0,1	18 ± 1	0,1 ± 0	38 ± 1	11,6 ± 0,6	0 ± 0	436 ± 38	464 ± 13
	B	57,2 ± 1,0	11,9 ± 0,5	15 ± 0	0,1 ± 0	28 ± 1	7,2 ± 0,4	0 ± 0	294 ± 23	510 ± 0
	C	55,7 ± 1,4	16,03 ± 3,8	16 ± 1	0,1 ± 0	29 ± 2	7,3 ± 0,6	0 ± 0	283 ± 25	510 ± 0
	D	80,4 ± 1,5	5,9 ± 0,3	20 ± 1	0,1 ± 0	45 ± 1	15,1 ± 0,5	0 ± 0	625 ± 15	369 ± 12
	E	67,7 ± 1,0	8,8 ± 0,6	17 ± 1	0,1 ± 0	37 ± 0	11 ± 0,4	0 ± 0	381 ± 49	476 ± 10

ID	TOC ($mg.g^{-1}$)	DOC ($mmol.l^{-1}$)	SUVA 254 ($L.mgC^{-1}.m^{-1}$)	E2/E3	a_{350} (m^{-1})	BIX	HIX	SR	FI	$S_{275-295}$
VKP-a	13.9 ± 0.9	0.5 ± 0.2	3.0 ± 0.8	4.5 ± 1.1	4.7 ± 1.9	1.5 ± 0.5	1.5 ± 0.8	1.5 ± 0.1	1.8 ± 0.2	0.016 ± 0.003
VKP-b	28.1 ± 1.0	0.5 ± 0.1	4.5 ± 1.1	4.5 ± 0.3	7.9 ± 0.1	1.3 ± 0.5	3.6 ± 2.4	1.1 ± 0.0	1.6 ± 0.0	0.015 ± 0.001
VKP-c	59.3 ± 2.1	0.8 ± 0.2	5.1 ± 0.8	3.4 ± 0.7	17.7 ± 4.3	0.8 ± 0.4	12.5 ± 11.3	1.4 ± 0.2	1.5 ± 0.1	0.014 ± 0.002
VKP-d	36.9 ± 5.0	0.7 ± 0.2	4.6 ± 0.4	3.7 ± 0.7	13.0 ± 5.7	1.3 ± 0.1	2.9 ± 0.3	1.3 ± 0.2	1.5 ± 0.0	0.014 ± 0.002
VKP-e	29.4 ± 1.7	0.4 ± 0.0	7.3 ± 1.2	3.2 ± 0.2	13.8 ± 1.5	0.7 ± 0.1	9.9 ± 3.1	1.2 ± 0.1	1.5 ± 0.1	0.013 ± 0.0
O-a	35.8 ± 1.3	0.6 ± 0.2	11.2 ± 2.8	2.9 ± 0.8	36.5 ± 28.5	0.6 ± 0.1	8.2 ± 1.9	0.9 ± 0.1	1.4 ± 0.1	0.01 ± 0.003
O-b	18.7 ± 1.4	0.3 ± 0.0	8.9 ± 4.0	2.9 ± 1.2	16.8 ± 11.1	2.1 ± 2.3	2.6 ± 1.9	0.9 ± 0.2	1.4 ± 0.0	0.01 ± 0.005
O-c	32.3 ± 6.4	0.7 ± 0.2	8.3 ± 2.4	3.1 ± 0.8	25.8 ± 6.4	0.7 ± 0.2	6.7 ± 2.6	1.3 ± 0.6	1.4 ± 0.1	0.012 ± 0.002
O-d	47.6 ± 2.0	2.2 ± 0.4	15.8 ± 2.3	2.2 ± 0.3	222.4 ± 34.5	0.8 ± 0.4	9.4 ± 6.1	0.8 ± 0.1	1.4 ± 0.0	0.007 ± 0.001
O-e	32.8 ± 2.4	0.6 ± 0.1	11.9 ± 2.4	1.6 ± 0.4	62.2 ± 22.4	0.9 ± 0.4	6.7 ± 4.7	0.8 ± 0.1	1.7 ± 0.2	0.004 ± 0.003
D-a	15.7 ± 5.6	0.3 ± 0.2	3.1 ± 1.5	2.5 ± 0.8	5.0 ± 1.4	1.2 ± 0.5	1.8 ± 0.5	2.7 ± 0.2	3.0 ± 0.8	0.01 ± 0.002
D-b	61.9 ± 2.3	0.6 ± 0.1	10.7 ± 1.0	1.4 ± 0.1	53.7 ± 10.9	0.7 ± 0.1	9.2 ± 1.7	1.0 ± 0.0	1.7 ± 0.1	0.004 ± 0.001
D-c	35.9 ± 1.5	0.4 ± 0.2	13.4 ± 7.1	1.2 ± 0.0	43.2 ± 9.1	0.8 ± 0.0	6.4 ± 1.7	1.4 ± 0.1	2.1 ± 0.1	0.003 ± 0.0
D-d	21.0 ± 0.8	0.5 ± 0.2	6.3 ± 2.3	1.2 ± 0.1	34.2 ± 19.3	0.9 ± 0.2	4.6 ± 3.1	2.1 ± 0.6	2.7 ± 0.8	0.003 ± 0.001
D-e	20.5 ± 1.5	0.3 ± 0.1	6.4 ± 1.4	1.3 ± 0.1	20.0 ± 4.2	0.8 ± 0.1	3.5 ± 0.3	1.6 ± 0.2	2.8 ± 0.1	0.004 ± 0.001
C-a	15.6 ± 2.4	0.2 ± 0.1	12.9 ± 9.0	1.4 ± 0.1	20.5 ± 10.5	1.1 ± 0.1	2.8 ± 0.3	1.6 ± 0.5	3.0 ± 0.3	0.004 ± 0.001
C-b	27.1 ± 6.9	0.2 ± 0.0	5.6 ± 3.5	3.1 ± 1.9	9.0 ± 8.6	1.1 ± 0.3	4.1 ± 1.7	1.3 ± 0.1	2.0 ± 0.2	0.011 ± 0.007
C-c	24.7 ± 1.5	0.3 ± 0.1	8.3 ± 1.9	1.3 ± 0.0	22.2 ± 5.9	2.8 ± 1.0	1.1 ± 0.7	1.3 ± 0.3	2.7 ± 0.1	0.003 ± 0.0
P-a	16.5 ± 4.9	0.3 ± 0.1	6.1 ± 2.0	1.9 ± 0.5	11.1 ± 2.5	1.0 ± 0.4	3.9 ± 2.9	1.2 ± 0.2	2.8 ± 1.0	0.006 ± 0.003
P-b	10.9 ± 1.8	0.3 ± 0.0	9.1 ± 6.1	2.9 ± 1.6	16.2 ± 12.2	1.0 ± 0.3	5.2 ± 3.2	1.5 ± 0.4	2.2 ± 0.7	0.011 ± 0.004
P-c	20.7 ± 2.2	0.2 ± 0.1	5.6 ± 1.3	3.6 ± 1.3	7.0 ± 5.2	0.8 ± 0.1	8.3 ± 0.6	1.3 ± 0.1	2.9 ± 1.1	0.013 ± 0.003

4 sites (VKP, Ouegoa, Dumbéa, South of Nouméa)				Previous study			
Component	Ex (nm)	Em (nm)	Type	Comp.	Ex (nm)	Em (nm)	References
C1	250	440-450	Humic-like	A	230-260	400-480	Coble (1996)
	330		Humic-like	M region	312	420/480	(Shank et al., 2010)
C2	235/305	353-356	Tryptophane-like	T1	220-235	334-360	Coble (1996)
C3	210	470-473	Fulvic acid	Region III	200-250	380-550	(Chen et al., 2003)
C4	270/385	483-486	Humic-like terrestrial		370-390	460-480	(Baker, 2001)(Baker, 2002)